



NUPR1 interacts with eIF2 α and is required for resolution of the ER stress response in pancreatic tissue

Maria Teresa Borrello¹ , Patricia Santofimia-Castaño¹, Marco Bocchio², Angela Listi¹, Nicolas Fraunhofer¹, Philippe Soubeyran¹, Eric Chevet³ , Christopher Pin^{1,4} and Juan Iovanna¹

¹ Centre de Recherche en Cancérologie de Marseille, INSERM U1068, CNRS UMR 7258, Aix-Marseille Université and Institut Paoli-Calmettes, Marseille, France

² INMED (INSERM U1249), Turing Center for Living Systems, Aix-Marseille University, Marseille, France

³ INSERM U1242, Proteostasis and Cancer Team, Chemistry Oncogenesis Stress Signaling, Université de Rennes 1, Rennes, France

⁴ Departments of Pediatrics, Oncology, and Physiology and Pharmacology, Schulich School of Medicine, University of Western Ontario, Children's Health Research Institute, London, ON, Canada

Keywords

eIF2 α ; ER stress; NUPR1; protein translation; unfolded protein response

Correspondence

M. T. Borrello and J. Iovanna, Centre de Recherche en Cancérologie de Marseille (CRCM), INSERM U1068, CNRS UMR 7258, Aix-Marseille Université and Institut Paoli-Calmettes, Parc Scientifique et Technologique de Luminy, 163 Avenue de Luminy, 13288 Marseille, France
 Tel: +33-491828803
 E-mail: maria-teresa.borrello@inserm.fr (MTB); juan.iovanna@inserm.fr (JI)

(Received 22 May 2020, revised 20 November 2020, accepted 4 January 2021)

doi:10.1111/febs.15700

Nuclear protein 1 (NUPR1) is a stress response protein overexpressed upon cell injury in virtually all organs including the exocrine pancreas. Despite NUPR1's well-established role in the response to cell stress, the molecular and structural machineries triggered by NUPR1 activation remain largely debated. In this study, we uncover a new role for NUPR1, participating in the unfolded protein response (UPR) and the integrated stress response. Biochemical results and ultrastructural morphological observations revealed alterations in the UPR of acinar cells of germline-deleted *NUPR1* murine models, consistent with the inability to restore general protein synthesis after stress induction. Bioinformatic analysis of NUPR1-interacting partners showed significant enrichment in translation initiation factors, including eukaryotic initiation factor (eIF) 2 α . Co-immunoprecipitation and proximity ligation assays confirmed the interaction between NUPR1 and eIF2 α and its phosphorylated form (p-eIF2 α). Furthermore, our data suggest loss of NUPR1 in cells results in maintained eIF2 α phosphorylation and evaluation of nascent proteins by click chemistry revealed that NUPR1-depleted PANC-1 cells displayed a slower post-stress protein synthesis recovery when compared to wild-type. Combined, these data propose a novel role for NUPR1 in the integrated stress response pathway, at least partially through promoting efficient PERK branch activity and resolution through a unique interaction with eIF2 α .

Introduction

Nuclear protein 1 (NUPR1), also known as p8 or Com1, is an intrinsically disordered protein first identified during the onset of pancreatitis [1]. We and others demonstrated NUPR1 is transiently induced in almost all organs and cells in response to a variety of injuries [2–6] including minimal stresses such as the renewal of

culture medium [7]. While it is clear NUPR1 acts as an essential element during the stress cell response, protecting cells from genotoxic or oxidative injury [8–11], the mechanisms by which NUPR1 acts still need to be elucidated. The highest expression of NUPR1 has been reported in pancreatic acinar cells following

Abbreviations

ATF4, activating transcription factor 4; ATF6, activating transcription factor 6; CHOP, C/EBP homologous protein; eIF2 α , eukaryotic initiation factor; ER, endoplasmic reticulum; GRP78, glucose-regulated protein 78; IRE1, inositol-requiring enzyme 1; ISR, integrated stress response; NUPR1, nuclear protein 1; PERK, PKR-like ER kinase; TPS, thapsigargin; Tun, tunicamycin; UPR, unfolded protein response; Zy, zymogen granules.

induction of pancreatitis. Acinar cells are highly enriched for endoplasmic reticulum (ER) due to their having the highest rate of protein synthesis among all cell types [12,13]. A major function of the ER involves folding and post-translational modification of secreted and integral membrane proteins. Also, the ER maintains homeostasis between folded and unfolded proteins [14,15] and disturbance of these physiological ER activities leads to a cell stress response implicated in a variety of pathological states [14,16,17]. Several pieces of evidence indicate that NUPR1 is involved in the onset of ER stress, but its role in this context remains largely unexplored [18,19].

Endoplasmic reticulum stress can be activated by a number of events including accumulation of unfolded proteins in the ER, subsequently triggering several signaling pathways that, together, are termed the unfolded protein response (UPR). The ultimate goal of the UPR is to resolve homeostatic imbalance between folded and unfolded proteins. If protein homeostasis is not restored, the UPR triggers apoptosis to safely dispose damaged cells. The UPR is comprised of three main branches—PKR-like ER kinase (PERK), inositol-required enzyme 1 (IRE1), and activation transcription factor 6 (ATF6). In the absence of stress, these molecules are bound to the chaperone BiP (glucose-regulated protein 78 or HSPA5). When excessive protein load occurs, BiP dissociates from PERK, IRE1, and ATF6 leading to their activation [20]. Activation of PERK leads to phosphorylation of the eukaryotic initiation factor 2 α (eIF2 α), which is a critical regulator of protein translation. Phosphorylated eIF2 α prompts a dramatic reduction in protein translation to limit cellular amino acid consumption. However, several mRNA transcripts elude the translation block, including activating transcription factor 4 (ATF4). ATF4 increases cell survival by promoting the expression of genes involved in protein folding, amino acid import, and biosynthesis of aminoacyl transfer RNAs [21]. When protein homeostasis is restored, GADD34/PPP1R15A, which is activated by ATF4, promotes eIF2 α dephosphorylation, thereby restoring normal protein synthesis [22]. Prolonged or excessive ER stress activation leads to programmed cell death, mainly mediated by the activation of the CCAAT/enhancer-binding protein (C/EBP) homologous protein (CHOP) [16,22], which promotes apoptosis via the intrinsic mitochondrial pathway.

The goals of this study were to examine whether the absence of NUPR1 altered the ER stress response and UPR in the pancreas and determine a possible mechanism by which NUPR1 affected this pathway. We report that NUPR1 constitutes an important element

of the UPR activation. Our data show that in the absence of NUPR1 in the pancreas, phosphorylation of eIF2 α is maintained, thereby preventing full recovery from ER stress response. We provide evidence that NUPR1s directly interacts with eIF2 α and that it may be required for its dephosphorylation. This novel function for NUPR1 links these two critical factors involved in the integrated stress response (ISR).

Results

Biochemical evaluation of ER stress activators in pancreatic acinar cells of *Nupr1*^{+/+} and *Nupr1*^{-/-} mice

Recently, we reported that pancreatic tissue from mice lacking *Nupr1* (*Nupr1*^{-/-}) have a significant downregulation in genes related to ER stress response [18]. This suggests that in the pancreas, NUPR1 could have a role in the UPR modulation. To verify this hypothesis, pharmacological activation of stress was initiated by a single injection of tunicamycin (Tun, 1.0 $\mu\text{g}\cdot\text{g}^{-1}$) in *Nupr1*^{-/-} and *Nupr1*^{+/+} mice. Tun induces ER stress by inhibiting protein *N*-glycosylation, thereby preventing correct protein folding [23]. Sixteen hours after Tun administration, whole pancreatic protein extracts were collected and the expression levels of the major UPR mediators of the PERK and IRE1- α branches were evaluated by western blot and qPCR (Fig. 1). PERK accumulation and phosphorylation appeared similar between the two genotypes (Fig. 1A,B). Consistent with the activation of PERK signaling, increased expression of ATF4 was observed in both *Nupr1*^{-/-} and *Nupr1*^{+/+} following activation of cell stress (Fig. 1A–B). However, the expression of ATF4 was reduced in *Nupr1*^{-/-} mice pancreata at protein and mRNA levels (Fig. 1A–C) compared with *Nupr1*^{+/+} following Tun injection ($P < 0.0001$). Reduced ATF4 was supported by the absence of CHOP protein expression in *Nupr1*^{-/-} mice (Fig. 1A,B). Interestingly, while we observed reduction in *Chop* mRNA in *Nupr1*^{-/-} mice compared with *Nupr1*^{+/+} (effect of Tun: $P < 0.0001$; effect of genotype: $P < 0.0001$; interaction: $P < 0.0001$; *Nupr1*^{+/+} vs *Nupr1*^{-/-} in Tun condition: $P < 0.0001$, *post hoc* Sidak's test, $n = 6$), an increase in *Chop* mRNA was still observed (Fig. 1C). *Gadd34* mRNA analysis, another target of UPR, also resulted lower in *Nupr1*^{-/-} pancreata compared with *Nupr1*^{+/+} after stress induction (Fig. 1C).

Phosphorylation of the eIF2 α (p-eIF2 α) is a critical event in the cellular stress response, mediating a transient protein synthesis shutoff. GADD34 is directly involved in eIF2 α dephosphorylation once the stress

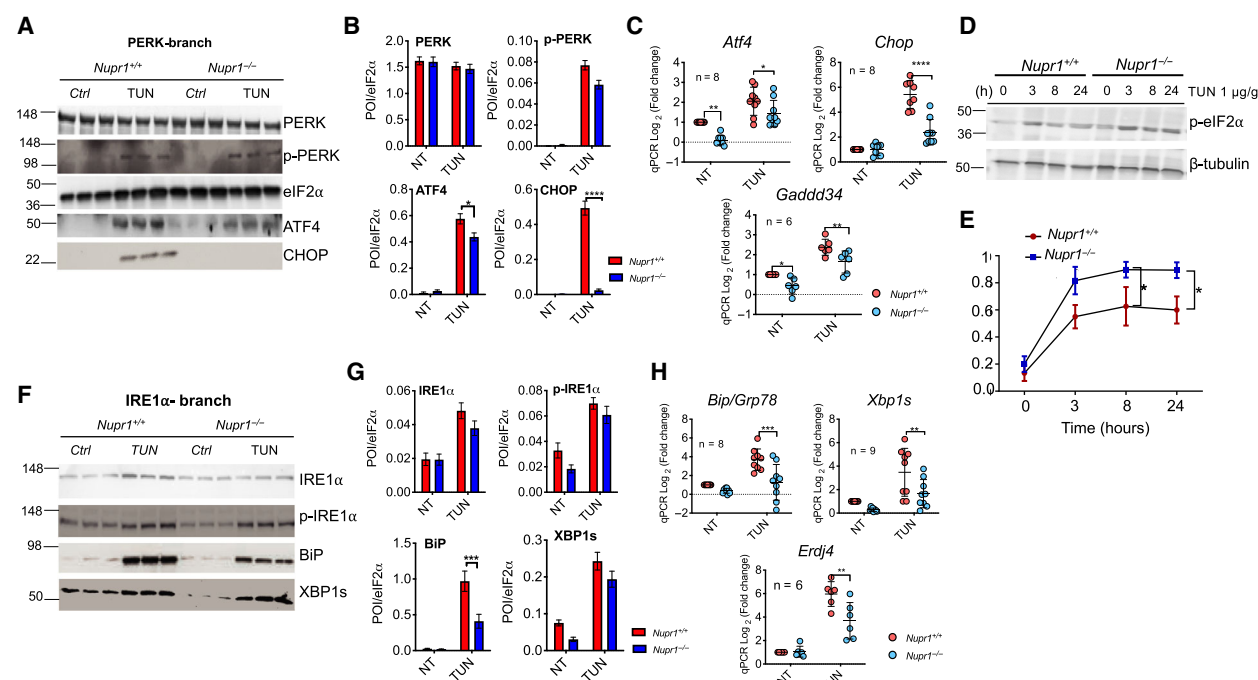


Fig. 1. Biochemical evaluation of ER stress-related proteins after Tun treatment in the pancreas. (A) Western blot of PERK, p-PERK, ATF4, eIF2 α , and CHOP of tissue lysates prepared from *Nupr1*^{+/+} and *Nupr1*^{-/-} mice pancreata upon 16-h injection with 1 μ g of Tun or vehicle (Ctrl, 150 mM of D-glucose). Image shows results from *N* = 3 mice per condition, but the experiment was replicated in *N* = 6 mice per condition in total. (B) represents the quantification of (A) using IMAGEJ software (Bethesda, MA, USA). Mean band intensity plotted \pm SD. Significant differences were calculated by two-way ANOVA with *post hoc* Sidak's test (*N* = 6). (C) RT-qPCR results of mRNA expression of *Atf4* and *Chop*, *Gadd34*. RNA was extracted from *Nupr1*^{+/+} and *Nupr1*^{-/-} mice upon 16-h injection with Tun or vehicle. Significant differences were calculated by two-way ANOVA with *post hoc* Sidak's test. The number of animals used for the evaluation of each gene is reported in the figure (*N* \geq 6). Statistically significant differences are shown (**P* < 0.03, ***P* < 0.001, *****P* < 0.0001). Error bars are mean \pm SD. (D) Western blot of p-eIF2 α of tissue lysed prepared from *Nupr1*^{+/+} and *Nupr1*^{-/-} pancreata after Tun injections over a period of time (0, 3, 8, 24 h). Experiment repeated in *N* = 3 mice. (E) Quantification of (D) using IMAGEJ software. Mean band intensity plotted \pm SEM (*N* = 3 mice); significant differences were calculated by two-way ANOVA with *post hoc* Sidak's test. (F) Western blot of IRE1 α , p-IRE1 α , BiP, and XBP1s of tissue lysates prepared from *Nupr1*^{+/+} and *Nupr1*^{-/-} pancreata upon 16-h injection with Tun or vehicle (Ctrl, 150 mM of D-glucose). Image shows results from *N* = 3 mice per condition, but the experiment was replicated in *N* = 6 mice per condition in total. (G) is the quantification of (F) using IMAGEJ software. Mean band intensity plotted \pm SD; significant differences were calculated with two-way ANOVA with *post hoc* Sidak's test. Statistically significant differences between *Nupr1*^{+/+} and *Nupr1*^{-/-} mice are shown (**P* < 0.02, ***P* < 0.01, ****P* < 0.001, *****P* < 0.0001). (H) RT-qPCR results of mRNA expression of *BiP*, *Atf6*, *Xbps*, and *Erdj4*. RNA was extracted from *Nupr1*^{+/+} and *Nupr1*^{-/-} mice upon 16-h injection with Tun or vehicle. Significant differences were calculated by two-way ANOVA with *post hoc* Sidak's test. The number of animals used for the evaluation of each gene is reported in the figure (*N* \geq 6). Statistically significant differences are shown (***P* < 0.001, ****P* = 0.001). Error bars are mean \pm SD.

stimuli terminate. Given reduced *Gadd34* mRNA expression, we next measured the levels of p-eIF2 α up to 24 h following Tun injection (Fig. 1D–E). Three hours following Tun treatment, similar levels of p-eIF2 α were observed in *Nupr1*^{+/+} and *Nupr1*^{-/-} mice. However, following 6 and 24 h of Tun treatment, the levels of p-eIF2 α were significantly higher in *Nupr1*^{-/-} tissue compared with wild-type counterpart, revealing a possible delay in the mechanism of ER stress cessation in *Nupr1*^{-/-}.

Biochemical examination of IRE1 α branch activation showed poststress accumulation of IRE1 α and

phospho(p) IRE1 α with no significant variation in both genotypes (Fig. 1F,G). However, western blot analysis showed pancreatic expression of the chaperone BiP almost halved in *Nupr1*^{-/-} mice compared with *Nupr1*^{+/+} mice. Expression of the *BiP* mRNA (Fig. 1H) showed a consistent downregulation in *Nupr1*^{-/-} mice compared with *Nupr1*^{+/+} littermates (*n* = 6). For both protein and mRNA, two-way ANOVA revealed a significant effect of Tun (*P* < 0.0001 for protein expression and *P* < 0.001 for mRNA). Subsequent comparisons uncovered a significant difference in BiP between *Nupr1*^{+/+} and *Nupr1*^{-/-}

mice after Tun administration ($P < 0.0001$ for protein and $P = 0.0228$ for mRNA, *post hoc* Sidak's test) but not in control conditions.

BiP is a stress sensor of the UPR and an integral part of the ER quality control system. Upon UPR initiation, the translational efficiency of BiP is normally increased by two- to threefold and it is regulated by several overlapping mechanisms [24]. Therefore, down-regulation of BiP protein and mRNA could be correlated with a faulty UPR machinery in *Nupr1*^{-/-} mice. Similar levels of total IRE1 α , p-IRE1 α , and spliced XBP1 (XBP1s) protein were observed in both *Nupr1*^{+/-} and *Nupr1*^{-/-}-treated mice, suggesting that an effective activation of the IRE1 α branch occurred. However, a significant difference was detected between the two genotypes when examining *Xbp1s* mRNA levels (Fig. 1H). The increase in *Xbp1s* mRNA induced by stress in *Nupr1*^{-/-} mice was significantly lower compared with *Nupr1*^{+/-} mice (effect of Tun: $P < 0.0001$; effect of genotype: $P = 0.003$, with no interaction between the two factors; *Nupr1*^{+/-} vs *Nupr1*^{-/-} in Tun condition: $P < 0.0001$; *post hoc* Sidak's test, $n = 6$). To validate the decrease in *Xbp1s* in *Nupr1*^{-/-} models, we evaluated *Erdj4* mRNA expression, a known target of XBP1s transcriptional regulation [25]. Consistent with reduced XBP1s function, *Erdj4* expression was decreased in *Nupr1*^{-/-} mice compared with the *Nupr1*^{+/-} littermates ($P = 0.001$, Fig. 1H).

Taken together, the results indicated that the loss of NUPR1 affects the normal buildup of events in the UPR pathway and, possibly, termination of ER stress.

NUPR1 deficiency could prevent initial ultrastructural alterations in murine pancreatic acinar cells after tunicamycin-induced cell stress

To determine the effects of deleting *Nupr1* on acinar cell morphology, we examined ultrastructural modifications of the ER in *Nupr1*^{+/-} and *Nupr1*^{-/-} mice 16 or 36 h post-Tun treatment using transmission electron microscopy. Representative micrographs indicate non-treated exocrine pancreatic cells (Fig. 2A,B) present with a normal ER, structurally ordered into thin, densely packed *cisternae* covered with ribosomes in both genotypes (arrows in insets of Fig. 2A,B). Overall, cell ultrastructure was normal in *Nupr1*^{-/-} mice. Acinar cells showed regular polarized organization with visible mononucleated cells (Nu) and electron-dense zymogen granules (zy). Sixteen hours post-Tun injection, acinar cells in *Nupr1*^{+/-} mice displayed dilated and expanded ER (Fig. 2C and inset) with an almost complete loss of associated ribosomes in the perinuclear area and fewer electron-dense zy. Expanded ER *cisternae* are a

cellular hallmark of the UPR as ER membranes expand to alleviate the stress due to an excessive load of misfolded proteins. Increasing ER volume decreases the relative concentration of unfolded protein intermediates, increases the time for protein folding, and avoids aggregate formation [26]. While a decrease in zy was detected in *Nupr1*^{-/-} pancreata (Fig. 2D), even 36 h after Tun treatment, little to no expansion of the ER was observed. As time progressed, damage to the ER was more aggravated in *Nupr1*^{+/-} mice, becoming fragmented (Fig. 2E). Such ER abnormalities were observed in *Nupr1*^{+/-} samples in more than 40% of the analyzed acinar cells (12/30 cells from 10 randomly selected fields of acquisition). Conversely, such ER dilation was almost completely absent in *Nupr1*^{-/-} samples (Fig. 2F).

The acinar cell phenotype observed in *Nupr1*^{-/-} mice suggests that translation of proteins may be generally affected in response to stress in these mice. Since an absence of NUPR1 is correlated with reduced *Gad65* expression and limited expansion of the ER in *Nupr1*^{-/-} mice, we speculated NUPR1 is required for restoration of protein synthesis. To test this hypothesis, acinar cells were isolated and assessed in culture (Fig. 3A). This process activates the UPR [27]. Morphological analysis of isolated acinar cells showed no obvious difference between *Nupr1*^{+/-} and *Nupr1*^{-/-} acini (Fig. 3B). Quantification of amylase levels, however, showed a significant decrease in amylase protein in *Nupr1*^{-/-} cells (Fig. 3C; $P < 0.05$, unpaired *t*-test), suggesting protein translation was reduced in these animals. It is possible, however, that lower amylase levels could reflect increased exocytosis in the absence of NUPR1. To examine this possibility, we measured secretion of amylase in *ex vivo* pancreatic acini from *Nupr1*^{+/-} and *Nupr1*^{-/-} mice (Fig. 3D). Following 30-min incubation with increasing concentrations of cerulein (analogue of cholecystokinin [28]) medium amylase levels revealed a dose-dependent response for both genotypes (Fig. 3D, effect of cerulein: $P < 0.012$, two-way ANOVA). Of note, amylase medium levels were significantly lower in *Nupr1*^{-/-} acinar cultures compared with *Nupr1*^{+/-} cultures (Fig. 3D, $P < 0.0001$, two-way ANOVA) supporting a model in which decreased amylase levels were due to either reduced synthesis or increased degradation in *Nupr1*^{-/-} acini.

Identifying the role of NUPR1 during ER stress response

Based on the observations so far, the loss of NUPR1 appears to affect restoration of protein synthesis in

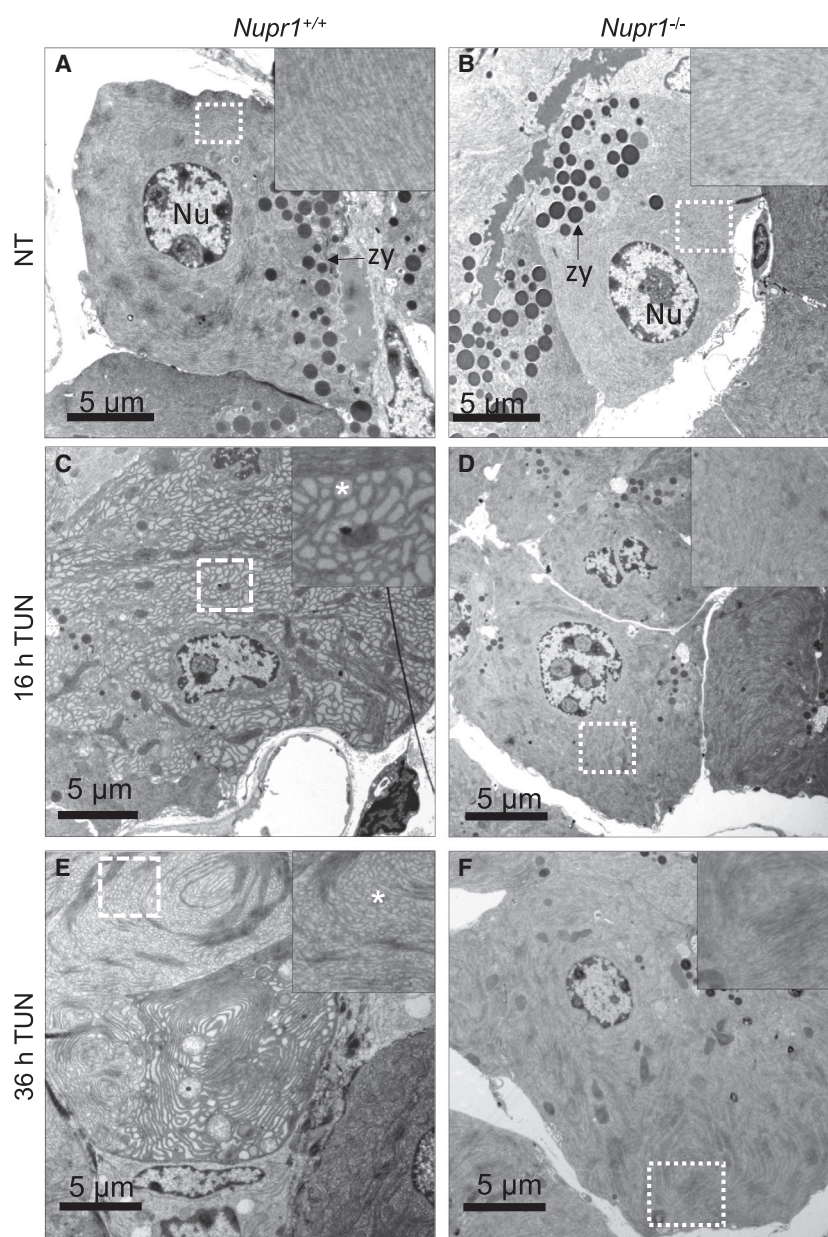


Fig. 2. Electron micrographs of *Nupr1*^{+/+} and *Nupr1*^{-/-} murine pancreata after ER stress induction with Tun (16 and 36 h). Representative transmission electron micrograph images of *Nupr1*^{+/+} and *Nupr1*^{-/-} pancreatic tissue of perfusion fixed mice injected IP with vehicle (NT, A and B and insets) or Tun (1.0 $\mu\text{g}\cdot\text{g}^{-1}$), at 16 (C and D) or 36 h (E and F) postinjection. Arrows point to the ER, and asterisks indicate dilated ER cisternae. Nu = nucleus. Results were replicated in $N = 2$ mice per condition ($N = 12$ mice in total). Scale bar information is reported in the figure.

response to ER stress. To identify the molecular mechanisms through which NUPR1 may regulate the UPR, we performed immunoprecipitation for NUPR1 to determine putative interacting proteins. Flag-tagged NUPR1 was expressed in MiaPaCa-2 cells and, as shown in Fig. 4A, the overexpression did not alter the rate of NUPR1 expression that occurred within physiological levels. Twenty-four hours post-transfection,

we performed immunoprecipitation for Flag either under normal conditions or following induction of ER stress by glucose starvation (GS) or addition of 1 μM thapsigargin (TPS); NUPR1-associated proteins were next identified by mass spectrometry (MS) resulting in 656 putative NUPR1-interacting proteins under normal conditions and 1152 or 828 interacting proteins under GS or TPS conditions (Fig. 4 and Tables S1–

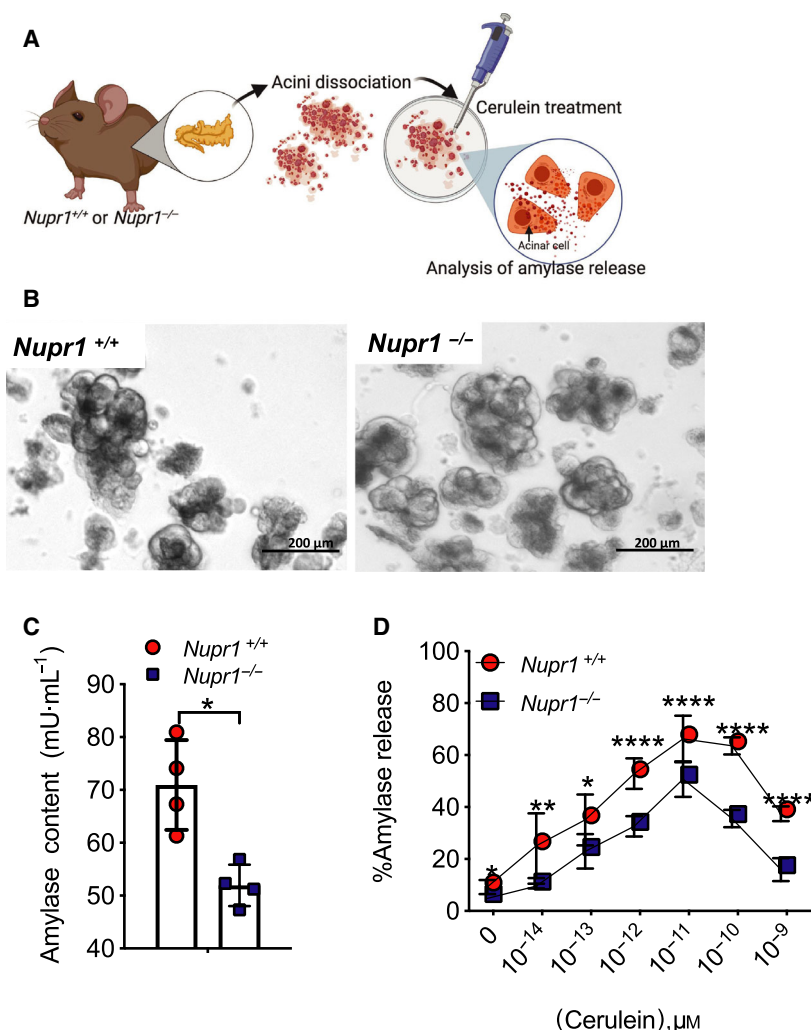


Fig. 3. Quantification of amylase content and amylase release levels in acinar cells isolated from *Nupr1*^{+/+} and *Nupr1*^{-/-} murine pancreata. (A) Dissociated acinar cells obtained from murine pancreata ($N = 8$ mice, 4 for *Nupr1*^{+/+} and 4 mice *Nupr1*^{-/-}) were incubated with increasing concentration of cerulein for 30 min. Amylase release onto the media was then measured. (B) Isolated acini from *Nupr1*^{+/+} or *Nupr1*^{-/-} mice. Experiment replicated in $N = 4$ mice per group. Scale bar information is reported in the figure. (C) Quantification of total amylase in *Nupr1*^{+/+} and *Nupr1*^{-/-} expressed in mU·mL⁻¹. Statistical significance was calculated with unpaired two-tailed t-test ($*P < 0.04$, $N = 4$ per group). Error bars represent mean \pm SD. (D) Amylase release from isolated *Nupr1*^{+/+} or *Nupr1*^{-/-} acinar cells following stimulation with increased concentrations of cerulein for 30 min. Statistical significance was measured with two-way ANOVA and *post hoc* Sidak's test for multiple comparisons ($*P < 0.01$, $**P < 0.014$, $****P < 0.0001$; $N = 4$ mice per group). Error bars represent mean \pm SD.

S3). Five hundred seventy-seven proteins were common to all conditions, with seven (nontreated), 365 (GS), and 77 proteins (TPS) specific to the various conditions. Bioinformatic analysis using the String protein–protein interaction database showed significant enrichment in translation initiation factors, supporting a model in which NUPR1 affects protein translation. Twenty-two out of a total of 142 proteins directly involved in translation initiation were identified under unstressed (nontreated) conditions ($P = 4.14 \times 10^{-7}$). As expected for a role in translation during cellular stress, the number of NUPR1-interacting proteins increased to 73 ($P = 5.19 \times 10^{-36}$) in GS and 45 ($P = 4.76 \times 10^{-21}$) in TPS-treated cells; this suggests an expanded role for NUPR1 in translational regulation during ER stress (Table S4).

The NUPR1 interactome included many translation initiation factors, which increased upon ER stress induction and included eIF2 α (eIF2S1), eIF2 β

(eIF2S2), and eIF2 γ (eIF2S3; Fig. 4C). These findings suggest a novel function for NUPR1 and provide a unique link between two important stress response proteins. Since our initial findings imply the levels of p-eIF2 α are increased in Tun-induced *Nupr1*^{-/-} acinar tissue, we decided to confirm this interaction. First, co-immunoprecipitation was performed following expression of a GFP-tagged NUPR1 in MiaPaCa-2 cells (Fig. 4D). The interaction between NUPR1 and eIF2 α was confirmed in nontreated cells showing that NUPR1 binds eIF2 α even under nonstressed conditions. Upon GS and TPS treatment, the interaction was maintained and even increased after TPS treatment, confirming MS data. Next, we performed the reverse co-IP, pulling down GFP-tagged NUPR1 using eIF2 α antibody (Fig. 4E). To show this interaction took place within the cell, the association between NUPR1 and p-eIF2 α /eIF2 α was examined using a proximity ligation assay (PLA, Duolink®, Sigma-

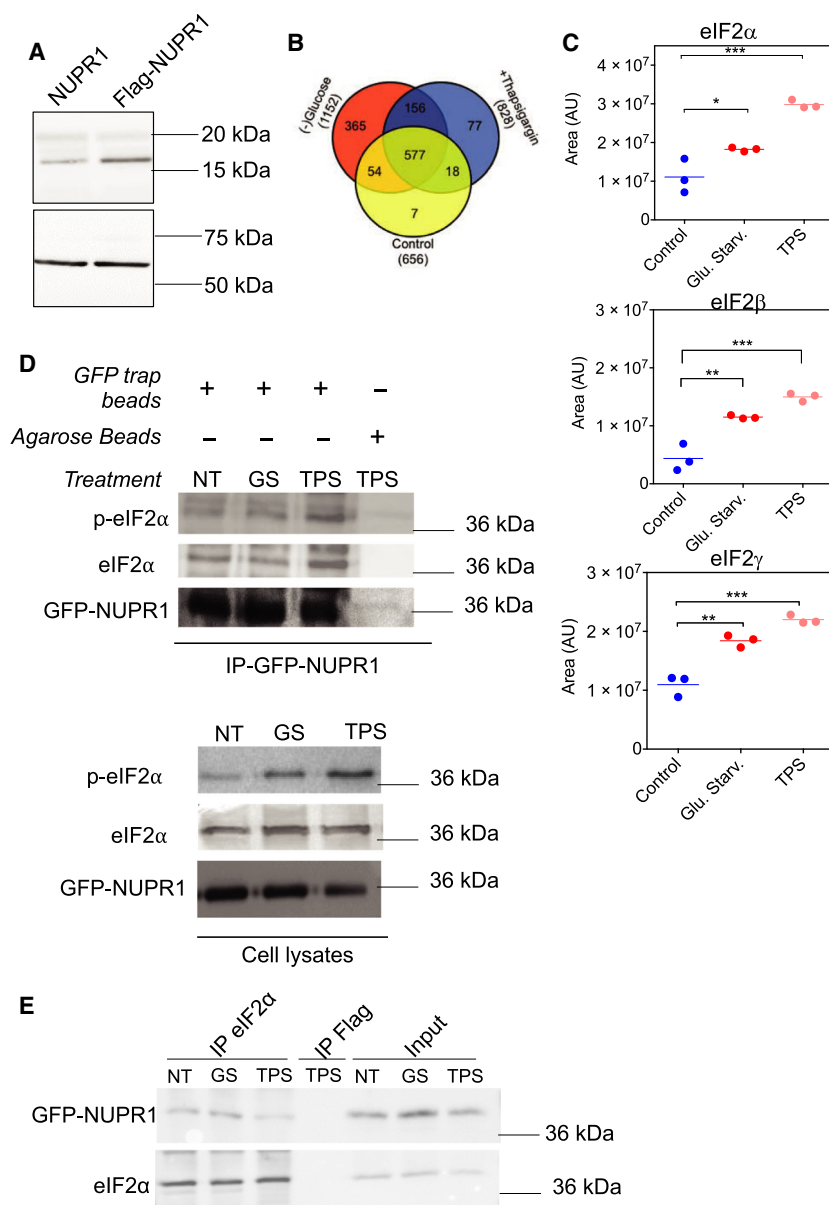


Fig. 4. Identification of putative NUPR1 interacting proteins. (A) Representative western blot for endogenous NUPR1 and transfected Flag-NUPR1 expression in MiaPaCa-2 cells used for co-immunoprecipitation analysis. (B) Venn diagram showing putative NUPR1-interacting proteins following GS or TPS (1 μ M, 24 h) treatment. (C) Quantification of MS peak areas of NUPR1-associated eIFs (n = 3, one-way ANOVA, * P = 0.02, ** P = 0.002, *** P = 0.0002). The figure reported is representative of three independent replicates. (D) Extracts from MiaPaCa-2 cells transiently transfected with GFP-NUPR1 were subjected to co-immunoprecipitation with GFP-Trap® beads or agarose beads followed by western blotting with the antibodies against p-eIF2 α and eIF2 α . Co-immunoprecipitation assay of GFP-tagged-NUPR1 confirm p-eIF2 α and eIF2 α interaction. (E) Co-immunoprecipitation of GFP-tagged-NUPR1 with eIF2 α demonstrates the reciprocal interaction is effective. The results reported are representative of three independent experiments.

Aldrich, Paris, France), which identifies molecular complexes that occur at distances <16 Å (Fig. 5). Confocal fluorescent microscopy analysis revealed PLA-positive foci under all conditions, suggesting NUPR1 interacts with eIF2 α independent of cell stress. Importantly, this interaction is extranuclear, which would be

expected for a direct interaction with eIF2 α and p-eIF2 α , and is the first direct evidence of an extranuclear function for NUPR1. PLA also revealed increased interaction following TPS treatment or GS, with NUPR1-eIF2 α and NUPR1-p-eIF2 α interactions remaining in the perinuclear area (Fig. 5D,F). These

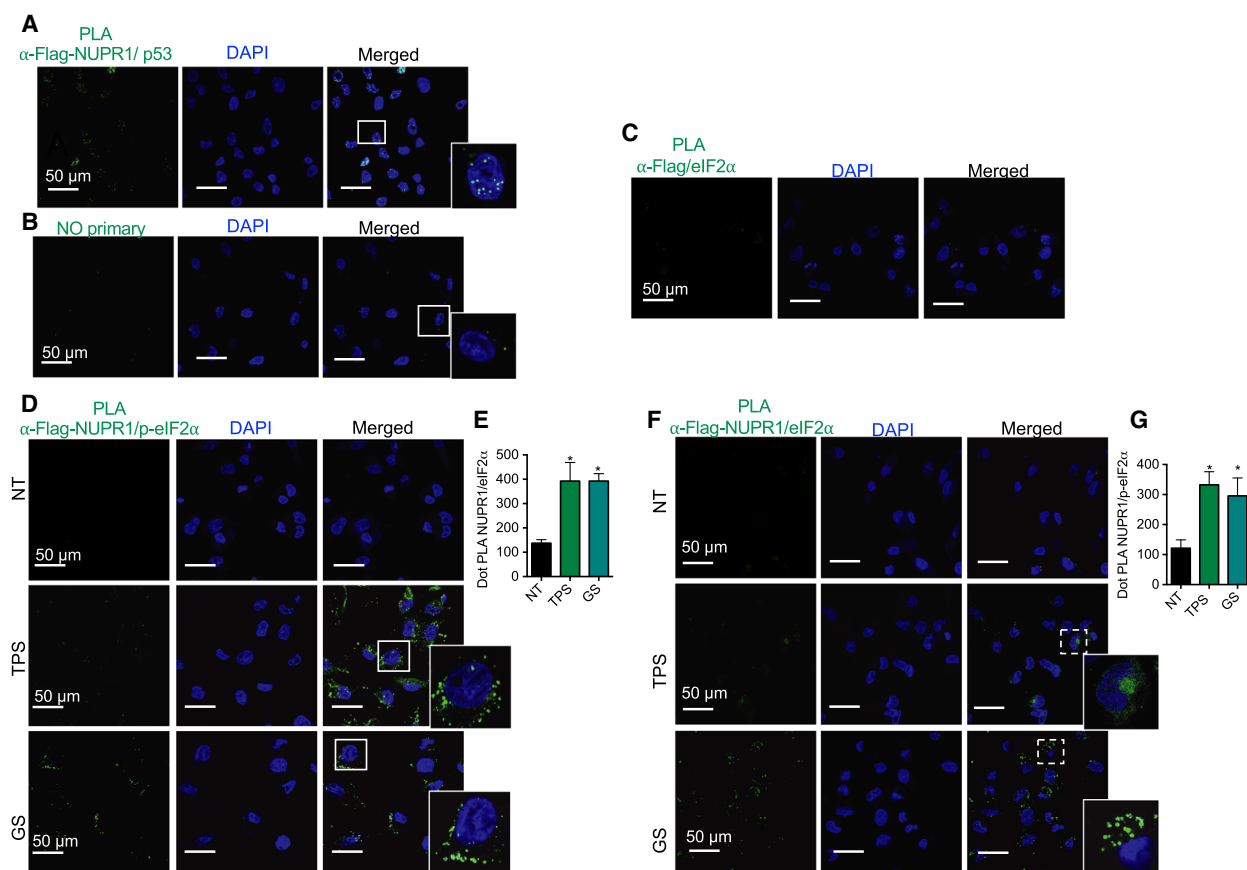


Fig. 5. *In situ* PLA between Flag-NUPR1 and eIF2 α /p-eIF2 α confirms the interaction of the proteins. Representative images of PLA experiment for Flag-NUPR1 and eIF2 α . (A–C) Controls experiments: (A) positive control PLA NUPR1 and p53; (B) PLA in the absence of primary antibody; (C) PLA in the absence of NUPR1 (MiaPaCa cells transfected with Flag empty vector); (D–G) Flag-NUPR1 and p-eIF2 α /eIF2 α were used to reveal interaction in control MiaPaCa-2 cells or following either TPS treatment (1 μ M) or GS for 24 h. (D, E) PLA assay to verify interaction with p-eIF2 α and quantification. (F–G) PLA assay to verify interaction with eIF2 α and quantification. Data are means of 10 fields each containing not < 150 nuclei. Statistical significance was calculated using ordinary one-way ANOVA values and corrected for multiple comparisons using Dunnett's *post hoc* test (* $P \leq 0.001$). Magnification 20 \times . Errors bars represent mean \pm SEM. All representative images illustrate results that were replicated in $N = 3$ separate experiments.

observations confirm that NUPR1 interacts with both eIF2 α and p-eIF2 α and ER stress increases or stabilizes the interaction.

NUPR1 depletion enhances eIF2 α phosphorylation and delays the translational recovery after stress induction

So far, our data revealed that NUPR1 interacts with eIF2 α in its both phosphorylated and unphosphorylated forms and this interaction may contribute to alleviating cell stress in acinar cells. The maintenance of high levels of p-eIF2 α in *Nupr1*^{−/−} acini propose models where NUPR1 would contribute directly or indirectly to the dephosphorylation of eIF2 α as a mechanism to allow restoration of protein translation.

To test this model, we examined phosphorylation of eIF2 α in response to ER stress response in PANC-1 cells (*NUPR1*^{+/+}) or NUPR1-null cells (*NUPR1*^{−/−}), generated by CRISPR/Cas9 deletion of *NUPR1* [29]. Treatment with 1 μ M of TPS for up to 24 h showed that *NUPR1*^{−/−} cells maintained higher levels of p-eIF2 α compared with *NUPR1*^{+/+} cells (Fig. 6A,B). These results prompted us to investigate whether the absence of NUPR1 interferes with the expression of downstream effectors of eIF2 α signaling, including CHOP and ATF4. Consistent with our *in vivo* pancreatic data, *NUPR1*^{−/−} cells showed delayed and reduced expression of ATF4 and CHOP compared with *NUPR1*^{+/+} cells, which show increased expression of these markers within 6 h of TPS treatment. RT-qPCR results confirmed reduced expression of both

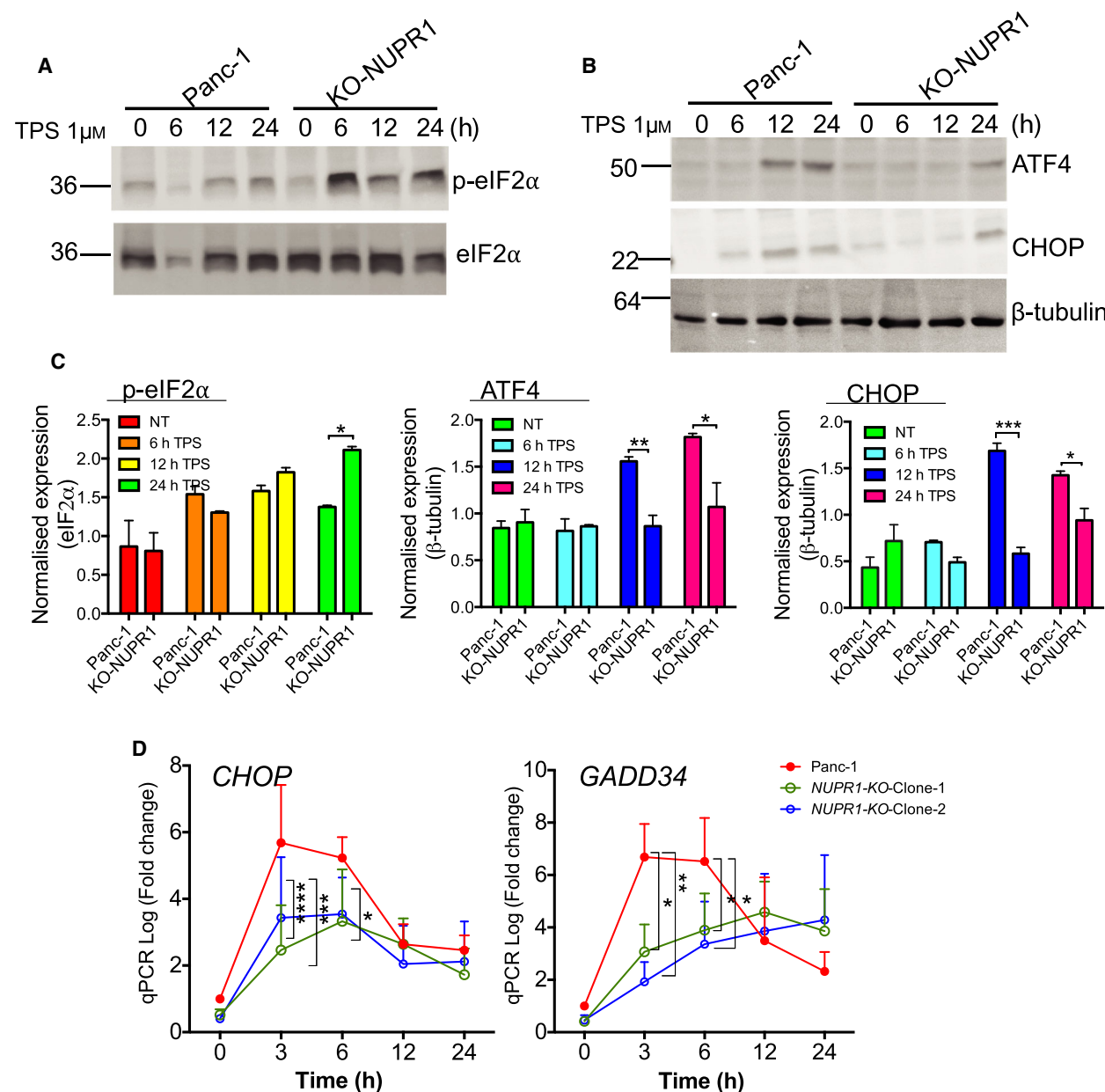


Fig. 6. eIF2 α phosphorylation in *NUPR1*-deficient and matched control PANC-1 cells in response to TPS induced ER stress. (A) Analysis of p-eIF2 α expression following 6, 12, and 24 h TPS treatment in protein extracts of PANC-1 cells with *NUPR1*^{+/+} (WT) or following CRISPR-Cas9-mediated deletion of *NUPR1*^{-/-} (KO-NUPR1). Results were replicated in *N* = 3 separate experiments. (B) Analysis of ATF4 and CHOP expression following 6, 12, and 24 h of TPS treatment in protein extracts of PANC-1 *NUPR1*^{+/+} or *NUPR1*^{-/-} cells (KO-Clone 1). Results were replicated in *N* = 3 separate experiments. (C) Quantification of A and B using IMAGEJ software. Mean band intensity plotted \pm SEM (*n* = 3). Significant differences were calculated by two-way ANOVA with *post hoc* Sidak's test (*n* = 3). (D) Analysis by RT-qPCR of *CHOP* and *GADD34* expression in *NUPR1*-deficient and matched control cells after treatment with 1 μ M TPS. Significant results between the two genotypes are reported in the graph (*****P* < 0.0001, ****P* < 0.001, ***P* = 0.0012, **P* = 0.04 at 3, 6, 12, and 24 h, respectively). The images reported for each panel are representative of three independent experiments.

CHOP and *GADD34* mRNAs at all time points in *NUPR1*^{-/-} cells (Fig. 6D), consistent with a deficit in PERK/eIF2 α signaling. At later stages of stress, *GADD34* participates in eIF2 α dephosphorylation to

revert the protein translation shutdown. The hindered expression of UPR markers such as *CHOP* and *ATF4* in *in vivo* and *in vitro* *NUPR1* loss-of-function models could be therefore a direct cause of a sustained

phosphorylation of eIF2 α . By expressing lower levels of GADD34 mRNA expression at all time points, it could be that NUPR1-depleted cells have a possible defect in the eIF2 α dephosphorylation process.

Sustained p-eIF2 α and low levels of GADD34 should affect protein synthesis recovery after stress induction. Therefore, to examine the restoration of normal protein synthesis in the absence of NUPR1, we induced the UPR for 1 h with TPS (1 μ M) in *NUPR1*^{+/+} and *NUPR1*^{-/-} PANC-1 clones and assessed the nascent proteins for up to 16 h later using *in situ* click chemistry (Fig. 7). To do this, cells were incubated with a puromycin analogue bearing a propargyl group for 1 h, allowing co-translational incorporation at the C terminus of nascent polypeptide chains. The incorporated propargyl puromycin forms an *in situ* covalent conjugate by copper-catalyzed click reaction with a fluorescently labeled azide (FITC azide). The reaction enables subsequent analysis of protein synthesis based on FITC fluorescence levels using confocal microscopy and cytometry [30].

NUPR1-depleted cells showed a slower translational recover after stress treatment as shown by a reduction in *de novo* protein synthesis at 3 and 16 h. At 3 h after TPS incubation withdrawal, *NUPR1*^{-/-} cells displayed lower levels of fluorescence compared with untreated cells (Fig. 7A–C, and quantification, Fig. 7D), suggesting reduced amount of nascent proteins. Decreased fluorescence was confirmed by two-way ANOVA, which showed an effect of both TPS ($P < 0.0001$) and NUPR1 ($P < 0.0001$), as well as an interaction between the two factors ($P = 0.001$; Fig. 7D). Six hours post-TPS treatment, *NUPR1*^{+/+} PANC-1 cells showed increased fluorescence, which is proportional to increased nascent protein synthesis. In line with sustained eIF2 α phosphorylation, both *NUPR1*^{-/-} clones maintained lower levels of fluorescence (Fig. 7D) until 16 h postpharmacological stress termination. Confocal results were confirmed at 6 h of TPS treatment by flow cytometry (Fig. 7E). Thus, our observations suggest a novel role for NUPR1 in modulating protein synthesis in response to cellular stress.

Discussion

NUPR1 is rapidly activated in response to a variety of stresses including several ER stress inducers such as serum starvation, cycloheximide, ceramide, staurosporine, and CCl₄ [2,4,6,19,31]. Until now, a direct role for NUPR1s within the UPR has not been identified. In this study, we identified a completely novel function for NUPR1 in directly interacting with eIF2 α /p-eIF2 α affecting the translational machinery

regulating ER stress and more broadly the ISR. *NUPR1*-deficient cells showed reduced expression of UPR markers and reduced protein synthesis compared with the wild-type counterpart following induction of stress both *in vivo* and *in vitro* models. This was combined with a lack of ER dilation, which is typically associated with re-activation of general translation and suggested that NUPR1 is required for restoring protein synthesis. Using global (MS) and targeted (co-IP, PLA) assays, we showed a novel and direct interaction between NUPR1 and eIF2 α , and show that this interaction occurs at the perinuclear regions of the cell. These findings constitute the first evidence of a direct, non-nuclear role for NUPR1 and are consistent with specific deficits observed in the absence of NUPR1, including reduced protein synthesis and ultrastructural differences in response to stress induction.

The UPR is a critical intracellular signaling pathway maintaining cellular homeostasis by finely tuning responses to various metabolic, oxidative, or inflammatory stresses [31]. A maladaptive UPR has been implicated in a variety of metabolic, neurodegenerative, and inflammatory diseases, as well as cancer. The main goal of an acute activation of UPR is to restore the ER homeostasis [12,32] and promote mechanisms directed to reducing misfolded proteins. These mechanisms include ubiquitination followed by proteasome degradation of misfolded proteins [33,34], autophagy [16,35], and the transitory arrest of protein synthesis and RNA processing that prevents accumulation of misfolded neoproteins into the ER [16,36]. Efficient activation of these mechanisms allows the cell to survive. Conversely, when these mechanisms are inadequate or sustained, ER-stressed cells initiate programmed cell death [16]. Using several complementary approaches, we have demonstrated that NUPR1 affects the recovery of protein synthesis during ER stress, at least in part, by associating with p-eIF2 α /eIF2 α and potentially promoting dephosphorylation of p-eIF2 α , thereby allowing restoration of normal protein synthesis. As a consequence, in *NUPR1*-deficient cells, protein synthesis is almost completely arrested correlating with prolonged phosphorylation of eIF2 α . Decreased eIF2 α activity would result in a reduced ER stress response. While we have not shown that NUPR1 interaction affects phosphorylation status of eIF2 α , the absence of NUPR1 leads to maintained p-eIF2 α and reduced protein synthesis, consistent with such a function.

However, it is likely that NUPR1's interaction with eIF2 α is not the only role it plays in the UPR and translation. The range of NUPR1-interacting partners identified by MS analysis suggests its potential

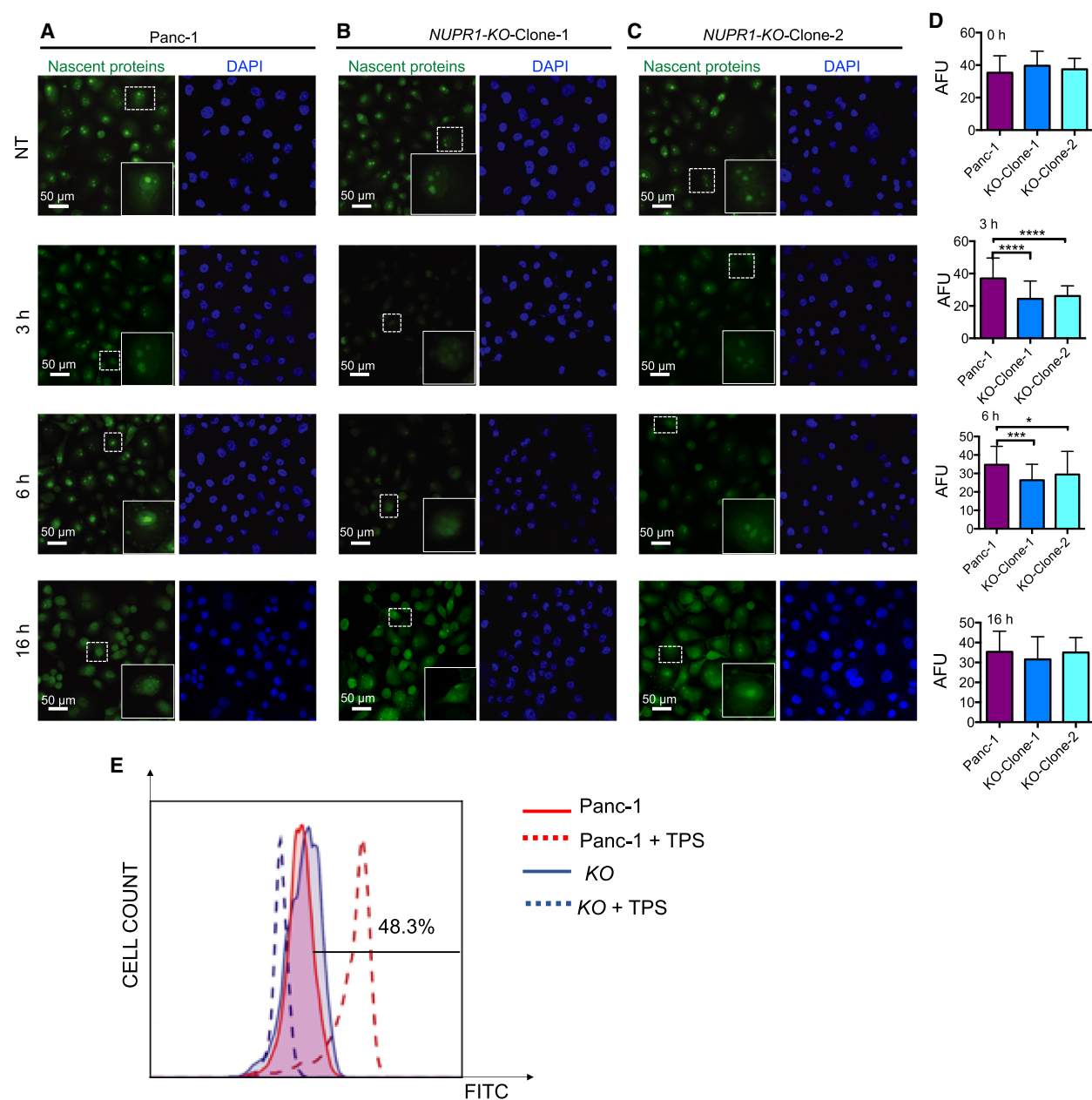


Fig. 7. NUPR1 deletion reduces nascent protein production in pancreatic cancer cells after stress induction. (A–C) Cultured PANC-1 cells or following CRISPR-Cas9-mediated deletion of *NUPR1* (*NUPR1*^{−/−} NUPR1-KO-Clone 1 and NUPR1-KO-Clone 2) was treated with vehicle or 1 μ M of TPS for 1 h. After 3–6 or 16 h, cells were incubated for 1 h with OP puromycin. Fluorescence was analyzed by confocal microscopy and arbitrary fluorescent intensity (AFU) measured with IMAGEJ. All representative images illustrate results that were replicated in *N* = 3 separate experiments. (D). Two-way ANOVA with a *post hoc* Dunnett test was used to determine statistical significance (**P* < 0.05, ****P* < 0.001, *****P* < 0.0001). (E) Flow cytometry of *de novo* protein synthesis measured with OP puromycin. Cells were gated based on forward scatter (FSC) and side scatter (SSC) parameters. The mean fluorescence increases are reported on the x-axis for WT or KO PANC-1 cells subjected to click chemistry of integrated OP puromycin conjugated with FITC azide. The y-axis represents the cell count. Errors bars represent mean \pm SEM. Scale bar information is reported in the figure.

functions in regulating numerous processes during cellular stress, including several transcriptional regulators, one of such functions could be indeed the

transcriptional regulation. Among all its interacting partners, we chose to focus on eIF2 α as it is a critical regulator that mediates the ISR. Upon ER stress

induction, the first cellular event in the UPR cascade involves eIF2 α phosphorylation that prompts a transient protein synthesis shutoff to re-establish the pre-stress proteostasis. In NUPR1-deficient cells, we observed an elevated and prolonged phosphorylation of eIF2 α associated with a reduced and delayed induction of UPR downstream effectors. The reduced expression and function of ATF4 (a direct regulator of *Chop* and *Gadd34* transcription) are somewhat surprising as *Atf4* generally escapes the translation block normally bestowed by p-eIF2 α . By interacting with eIF2 α , NUPR1 targets the translational initiation complex, which is important for the translation of ATF4 mRNA. Therefore, the expression of ATF4 is blunted, as well as CHOP expression and consequently *Gadd34* expression.

However, it is likely that NUPR1 deficiency affects multiple factors within the UPR, including ATF4, possibly through transcriptional mechanisms. Indeed, we observed deficits in IRE1 signaling suggesting a more widespread effect of NUPR1 deficiency on the UPR. Another possible mechanism involves GADD34. In the later stages of the ER stress response, GADD34 promotes the dephosphorylation of eIF2 α , thereby creating a negative feedback loop to release the transient protein synthesis block. Loss of GADD34 has been previously associated with a prolonged interruption in protein synthesis [32] and decreased expression of UPR downstream regulators. However, our MS data did not demonstrate a direct interaction of NUPR1 with GADD34 and we choose to focus on NUPR1 interacting proteins only (the ones that has been found associated with it in our co-IP experiments). NUPR1, in addition to association with the translational complex could potentially contribute to the regulation of eIF2 α phosphorylation through direct interaction with proteins involved in eIF2 α phosphorylation and

dephosphorylation. However, the exact mechanism warrants further investigation. While our data demonstrate NUPR1 functions influence translation through interacting with factors involved in translation initiation and regulation, it is likely that NUPR1 affects the UPR through multiple mechanisms.

In conclusion, our findings demonstrate a novel role for NUPR1 during ER stress. NUPR1 participates in the regulation of the UPR and more broadly to the ISR by participating in the transcriptional regulation by interacting with eIF2 α (Fig. 8). Collectively, our data support an essential role of NUPR1 in ER stress.

Materials and methods

Study approval

All experimental protocols were carried out in accordance with the nationally approved guidelines for the treatment of laboratory animals. All experimental procedures on animals were approved by the Comité d'éthique de Marseille numéro 14 (C2EA-14) in accordance with the European Union regulations for animal experiments.

Mouse strains and tissue collection

For all the *in vivo* experiments, we used *Nupr1*^{-/-} mice bear a homozygous deletion of exon 2 [33]. Mice were used between the 5 and 16 weeks of age, and as control, we used their mating littermates. Animals were kept in the Experimental Animal House of the Centre de Cancérologie de Marseille of Luminy. After sacrifice by cervical dislocation, pieces of pancreas were collected and frozen in cold isopentane for further analysis or directly homogenized in 4 M guanidine isothiocyanate lysis buffer for efficient pancreatic RNA extraction according to Chirgwin *et al*'s procedure [34].

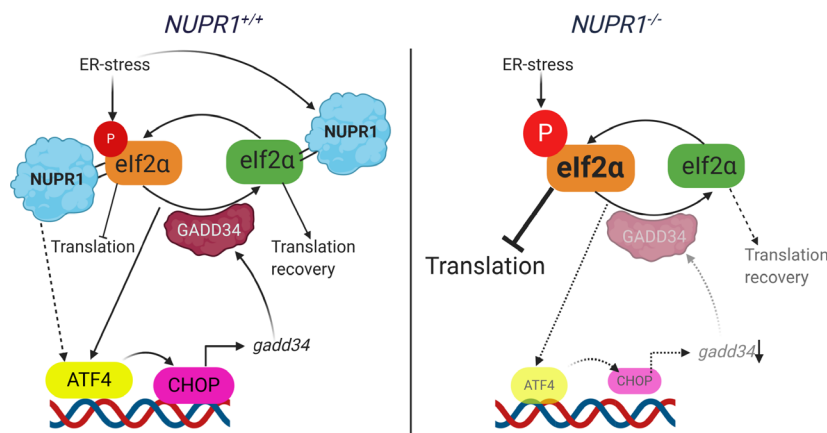


Fig. 8. NUPR1 interacts with eIF2 α and is required for resolution of the ER stress response in pancreatic tissue. NUPR1 by interacting with the eIF2 α participates in the translational regulation after stress. In the absence of NUPR1, the phosphorylation of eIF2 α is maintained for longer and the expression of downstream regulators of ER such as ATF4, CHOP, and *gadd34* blunted. The restoration of normal protein synthesis in the absence of NUPR1 is therefore delayed.

Tunicamycin injections

Mice of 5–8 weeks of age were injected intraperitoneally (IP) with 1 $\mu\text{g}\cdot\text{g}^{-1}$ of Tun (Sigma-Aldrich, Paris, France) using 150 mM of D-Glucose as vehicle. After the reported time point (up to 36 h), mice were sacrificed and organs were collected.

Cell culture

MiaPaCa-2 and PANC-1 cells were purchased from ATCC (Manassas, VA, USA) and cultures in Dulbecco's modified Eagle's medium (DMEM; Gibco, Life Technologies, Carlsbad, CA, USA), supplemented with 10% FBS (Lonza, Basel, Switzerland), and cultured at 37 °C and 5% CO₂. Cells were used in all experiments below 20 passages.

Preparation of protein lysates and western blotting

Forty milligram of frozen tissue was cut on dry ice and homogenized with Precellys® (Bertin instruments, Montigny-le Bretonneux, France) in 300 μL of ice-cold RIPA buffer [10 mM Tris/Cl (pH 8.0), 1 mM EDTA, 0.5 mM EDTA, 1% Triton X-100, 0.1% sodium deoxycholate, 0.1% SDS, 140 mM NaCl], complemented with 0.5 $\mu\text{g}\cdot\text{g}^{-1}$ of protease inhibitor kit (Sigma Aldrich, Paris, France), 200 μM of Na₃VO₄, 1 mM of PMSF, and 40 mM of β -glycerophosphate. After homogenization, the supernatant was cleared by centrifugation for 30 min at 12 000 *g* at 4 °C. Protein lysate content was quantified by micro BCA assay (Thermo Fisher Scientific, Illkirch-Graffenstaden, France), and 40 μg of protein was resolved by SDS/PAGE, transferred to nitrocellulose membrane for 1 or 2 h. Membranes were next blocked with Tris-buffered saline (TBS) in 5% BSA and blotted overnight with primary antibody (1 : 500 dilution in TBS 5% BSA). After washes, the membrane was incubated with HRP-conjugated secondary antibody (Boster, Pleasanton CA, USA) for 1 h at room temperature (1 : 5000 dilution in TBS 5% BSA). Subsequently, the membrane was washed and revealed with enhanced chemoluminescence. Chemiluminescent signal was detected in a G-Box (Syngene, Cambridge, Europe). The following antibodies were used: rabbit monoclonal ATF4 (D4B8), mouse monoclonal CHOP (L63F7), rabbit monoclonal XBP1s (E9V3E), rabbit monoclonal, BiP (C50B12), rabbit monoclonal eIF2 α XP® (D7D3), rabbit monoclonal Phospho-eIF2 α XP® (Ser51; D9G8), and rabbit monoclonal Phospho-PERK (Thr980) were obtained from Cell Signaling Inc. Technology (MA, USA) (G.305.4); rabbit polyclonal antibody Phospho-IRE1 α (Ser724; PA1-16927) is obtained from Thermo Fisher; and mouse monoclonal β -actin (#A5316) is obtained from Sigma-Aldrich (Paris, France). Quantification of signal was performed using IM-AGEJ software (NIH, Wisconsin, USA). Mean band

intensity was plotted over the intensity of eIF2 α \pm SEM ($n = 3$), and unpaired Student's *t*-test was used for statistical analysis.

Preparation of RNA and RT-qPCR

RNA from murine pancreata was extracted after 16 h of intraperitoneal injections of Tun following the Chirgwin procedure [34]. Total RNA from cells was obtained using RNeasy Kit (Qiagen, Paris, France) following manufacturer's instruction. The RNA integrity was assessed with Agilent 2100 Bioanalyzer with the RNA 6000 Nano Chip Kit. The RNAs were reverse-transcribed using GO Script Kit (Promega, Madison, WI, USA) following manufacturer's instruction. RT-qPCRs were performed using Aria Mix using Promega reagents. Primer sequences are described in Table 1. mRNAs were quantified relative to *Rpl0*. Data are presented in the graphs as log fold change compared with *Nupr1*^{+/+} controls (mice IP injected with vehicle, 150 mM D-Glucose) levels of expression. Significant differences were calculated using two-way ANOVA with *post hoc* Sidak's test ($N \geq 6$).

Transmission electron microscopy

Mice were perfused with 4% cold PFA and 2.5% glutaraldehyde. Pancreatic tissue was then immersed overnight in 0.1 M Sorensen buffer, postfixed in 1% osmium tetroxide, and in bloc-stained with 3% uranyl acetate. The tissue was dehydrated with increasing concentrations of ethanol on ice and acetone before being embedded in Epon. Ultrathin sections (70 nm) were prepared using a Leica UCT Ultramicrotome (Leica, Vienna, Austria) and stained with uranyl acetate and lead citrate and deposited on formvar-coated slot grids. The grids were observed in an FEI Tecnai G2 at 200 KeV, and acquisition was performed on a Veleta camera (Olympus, Tokyo, Japan).

NUPR1 expression vector transfection

MiaPaCa-2 cells were seeded in 12-well plates and transfected with 3 μg of DNA (NUPR1-GFP, NUPR1-Flag, or control vector) and 3 μL of Lipofectamine 3000 Transfection Reagent (Thermo Fisher Scientific) per well. Cells were assayed after 24 h post-transfection.

Co-immunoprecipitation

MiaPaCa-2 cells, expressing GFP-NUPR1, were plated in 10-cm² dishes. When reached, 80% confluence was treated with either 1 μM of TPS or glucose-starved (GS) for 24 h. After that time, cells were lysed on ice by using HEPES-based lysis buffer containing protease inhibitor cocktail (1 : 200; Sigma-Aldrich P8340). Lysates were cleared for

Table 1. Primer sequence.

Gene		5'–3' sequence	Accession Number
Sequence primers <i>Mus musculus</i>			
<i>Bip</i>	F	GGTGCAGCAGGACATCAAGTT	NC_000068.7
	R	CCCACCTCCAATATCAACTTGA	
<i>Chop</i>	F	CTGCCTTTCACCTTGGAGAC	NC_00076.6
	R	CGTTTCCTGGGGATGAGATA	
<i>Atf4</i>	F	ATGGCCGGCTATGGATGAT	NM_0097163
	R	CGAAGTCAAACCTTTTCAGATCC	
<i>Xbp1s</i>	F	GAGTCCGCAGCAGGTG	NM_013842
	R	GTGTCTAGAGTCCATGGGA	
<i>Erdj4</i>	F	TAAAAGCCCTGATGCTGAAGC	NM_013760.4
	R	TCCGACTATTGGCATCCGA	
<i>Rpl0</i>	F	GGCGACCTGGAAGTCCAAC	NM_007475
	R	CCATCAGCACCACAGCCTTC	
Sequence primers of <i>Homo sapiens</i>			
<i>GADD34</i>	F	GAGGAGGCTGAAGACAGTGG	NM_014330
	R	AATTGACTTCCCTGCCCTCT	
<i>CHOP</i>	F	GCCAGAGAAGCAGGGTCAAG	NM_004083
	R	GGAGCTGGAAGCCTGGTATG	
<i>RPL0</i>	F	GGCGACCTGGAAGTCCAAC	NM_001002
	R	CCATCAGCACCACAGCCTTC	

10 min at 14 000 r.p.m. at 4 °C, and protein concentration of the supernatant was determined by using protein assay (Bio-Rad). The co-immunoprecipitation was performed using GFP-Trap® beads (ChromoTek, GmbH, Munich, Germany) following manufacturer's protocol or rabbit monoclonal antibody specific for eIF2 α XP® (D7D3). Immunoprecipitates were pelleted, and washed with lysis buffer three times and then with PBS. The resultant proteins were denatured and blotted against eIF2 α , p-eIF2 α , and anti-GFP. To perform the reverse co-IP, MiaPaCa-2 cells expressing Flag-NUPR1 or Flag-GFP were grown to 70% confluence and treated as described above. Cells were lysed on ice using HEPES-based lysis buffer containing 10 mM NEM (*N*-Ethylmaleimide; Sigma, 04259) and a proteases inhibitor cocktail (1 : 200; Sigma, P8340). Lysates were centrifuged for 10 min at 14 000 r.p.m. at 4 °C. Protein concentration of the supernatant was determined using protein assay (Bio-Rad, Marnes-la-Coquette, France), and equal amounts of protein were incubated with 30 μ L of anti-Flag M2-coated beads under rotation for 2 h at 4 °C. Beads were then washed three times with cold lysis buffer, and proteins were eluted using 250 μ L ammonium hydrogen carbonate buffer containing 0.1 μ g μ L⁻¹ of Flag peptide for 90 min at 4 °C while rotating. After a short spin, the supernatant was recovered by using a Hamilton syringe. Eluted proteins were collected and analyzed by MS.

Click chemistry and fluorescence detection

PANC-1 and modified PANC-1 cells were grown on glass coverslips in DMEM supplemented with 10% FBS. Cells were treated with 1 μ M TPS for 1 h and then incubated in

fresh media without TPS. After 3, 6, or 16 h, *O*-propargyl puromycin (OP-puro) was added to cells in complete culture medium for 1 h. Cells were then washed with PBS and fixed with 4% PFA in PBS, after fixation cells were permeabilized with 0.3% Triton X-100 in PBS. Following removal of detergent by PBS washes, CuAAC detection of OP-puro incorporated into nascent protein was performed by reacting the fixed cells for 1 h at room temperature with 20 μ M FITC azide, as previously described [35]. After the click chemistry reaction, coverslips were washed several times with TBST, counterstained with Hoechst, and mounted in standard mounting media. The stained cells were imaged by LSM 510 META confocal microscope (Zeiss, Oberkochen, Germany) and on a Nikon Eclipse 90i Fluorescence Microscope. Stained cells were also quantified by flow cytometry in a MACSQuant-VYB (Miltenyi Biotec, Surrey, UK). Data analysis was carried out by using the FLOWJO LLC software (Ashland, Oregon, USA). The intensity of the fluorescent OP-puro stain in single cells was quantified by IMAGEJ. Statistical significance was calculated by using two-way ANOVA and corrected for Sidak's test.

Proximity ligation assay

MiaPaCa-2 transfected with Flag-NUPR1 were treated with TPS (1 μ M), or GS. After the indicated time points, cells were washed twice in PBS, fixed, washed twice again, permeabilized in PBS/0.1% Triton X-100, and saturated with blocking solution for 30 min before immune staining with the Duolink by using PLA Technology (Sigma-Aldrich, Paris, France) following the manufacturer's protocol. Slides were processed for *in situ* PLA by using

sequentially the Duolink *in situ* Detection Reagents Green, Duolink *In Situ* PLA Probe Anti-Mouse MINUS, and Duolink *In Situ* PLA Probe Anti-Rabbit PLUS (Sigma-Aldrich, Paris, France). The following antibodies were used: rabbit monoclonal eIF2 α -XP® (D7D3, from Cell Signaling Technology, Danvers, MA, USA), rabbit monoclonal Phospho-eIF2 α XP® (Ser51; D9G8, from Cell Signaling Technology), and mouse monoclonal antibody anti-FLAG M2 (from Sigma-Aldrich, Paris, France). In these experiments, green fluorescence corresponds to the PLA-positive signal, and it indicates that the two molecules belong to the same protein complex. Blue fluorescence corresponds to nuclei (so-called DAPI staining). Protein over-expression was used to obtain a clearer and better signal. Preparations were mounted using Prolong Gold Antifade Reagent (Invitrogen, Carlsband, CA, USA), and image acquisition was carried out on an LSM 510 META confocal microscope (Zeiss, Oberkochen, Germany) and on a Nikon Eclipse 90i Fluorescence Microscope.

Mass spectrometry analysis

Protein extracts were loaded on NuPAGE 4–12% Bis/Tris acrylamide gels according to the manufacturer's instructions (Invitrogen). Running was stopped as soon as proteins stacked in a single band. Protein-containing bands were stained with Imperial Blue (Pierce, Waltham, MA, USA), cut from the gel, and digested with high sequencing grade trypsin (Promega) before MS analysis [36].

MS analysis was carried out by LC-MS/MS using an LTQ-Velos-Orbitrap or a Q Exactive Plus Hybrid Quadrupole-Orbitrap (Thermo Electron, Bremen, Germany) coupled online with a nanoLC UltiMate 3000 RSLC Chromatography System (Dionex, Sunnyvale, CA, USA). Five microliters corresponding to 1/5 of the whole sample was injected in triplicate on the system. After sample pre-concentration and washing on a Dionex Acclaim PepMap 100 C18 Column (2 cm \times 100 μ m i.d. 100 Å, 5 μ m particle size), peptides were separated on a Dionex Acclaim PepMap RSLC C18 Column (15 cm \times 75 μ m i.d., 100 Å, 2 μ m particle size) at a flow rate of 300 nL·min⁻¹, a two-step linear gradient (4–20% acetonitrile/H₂O; 0.1% formic acid for 90 min and 20–45% acetonitrile/H₂O; 0.1% formic acid for 30 min). For peptide ionization in the nanospray source, voltage was set at 1.9 kV and the capillary temperature at 275 °C. All samples were measured in a data-dependent acquisition mode. Each experiment was preceded by a blank run to monitor system background. The peptide masses were measured in the LTQ-Velos-Orbitrap in a survey full scan (scan range: 300–1700 m/z , with 30 K FWHM resolution at m/z = 400, target AGC value of 1.00×10^6 , and maximum injection time of 200 ms). In parallel to the high-resolution full scan in the Orbitrap, the data-dependent CID scans of the 10 most intense precursor ions were fragmented and measured in the linear ion trap

(normalized collision energy of 35%, activation time of 10 ms, target AGC value of 1×10^4 , maximum injection time 100 ms, and isolation window 2 Da). Parent masses obtained in Orbitrap analyzer were automatically calibrated on 445.1200 locked mass. Dynamic exclusion was implemented with a repeat count of 1 and exclusion time of 30 s.

In the Q Exactive Plus Hybrid Quadrupole-Orbitrap, the peptide masses were measured in a survey full scan (scan range: 375–1500 m/z , with 70 K FWHM resolution at m/z = 400, target AGC value of 3.00×10^6 , and maximum injection time of 100 ms). Following the high-resolution full scan in the Orbitrap, the 10 most intense data-dependent precursor ions were successively fragmented in higher energy collisional dissociation cell and measured in Orbitrap (normalized collision energy of 25%, activation time of 10 ms, target AGC value of 1.00×10^3 , intensity threshold 1.00×10^4 maximum injection time 100 ms, isolation window 2 m/z , 17.5 K FWHM resolution, scan range of 200–2000 m/z). Dynamic exclusion was implemented with a repeat count of 1 and exclusion time of 20 s.

Mass spectrometry data analysis

Raw files generated from MS analysis were processed using Proteome Discoverer 1.4.1.14 (Thermo Fisher Scientific). This software was used to search data via in-house Mascot server (version 2.3.0; Matrix Science, London, UK) against the Human database subset of the SwissProt database (version 2017.03, 20184 human entries). A database search was done by using the following settings: a maximum of two trypsin miscleavage allowed, methionine oxidation and protein *N*-acetylation as dynamic modifications, and cysteine carbamidomethylation as fixed modification. A peptide mass tolerance of 6 p.p.m. and a fragment mass tolerance of 0.8 Da were allowed for search analysis. Only peptide identified with a FDR < 1% was used for protein identification.

To calculate the confident score (from 0 to 100%) for NUPR1-interacting proteins identified by MS, we used a formula derived from Bonacci *et al.* [37] based on peptide number count: K = total peptide number in control IP; V = total peptide number in NUPR1 IP; $\text{Conf} = ((2V)^2 / (1 + (2V) + (2K)^2) * 100 - 100 / (1 + (2(V - K))))$; = 0 if < 0; and values above 50 are usually considered to be confident.

Acknowledgements

The work was supported by La ligue Contre le Cancer, INCa, Canceropole PACA and INSERM (JI), and the Canadian Institutes of Health Research (MOP#PJT166029; CP). The electron microscopy experiments were performed in the PiCSL-FBI core facility (IBDM, AMU-Marseille). We thank Prof. Boaz Tirosh for the advice on the work and the

experiments. We thank the reviewers for the useful comments during the revision process.

Conflict of interest

The authors declare no conflict of interest.

Author contributions

MTB performed experiments, interpreted the data, and wrote the manuscript. PS-C performed experiments. MB assisted with histological preparations and analyzed the data. AL performed experiments under the supervision of MTB. NF commented on the manuscript. PS helped with interactome analysis. EC helped with data interpretation, CP supervised the project, designed the experiments, and wrote the manuscript. JI designed the study, supervised the project, interpreted the data, and wrote the manuscript.

Peer Review

The peer review history for this article is available at <https://publons.com/publon/10.1111/febs.15700>.

References

- Mallo GV, Fiedler F, Calvo EL, Ortiz EM, Vasseur S, Keim V, Morisset J & Iovanna JL (1997) Cloning and expression of the rat p8 cDNA, a new gene activated in pancreas during the acute phase of pancreatitis, pancreatic development, and regeneration, and which promotes cellular growth. *J Biol Chem* **272**, 32360–32369.
- Grasso D, Garcia MN, Hamidi T, Cano C, Calvo E, Lomberg G, Urrutia R & Iovanna JL (2014) Genetic inactivation of the pancreatitis-inducible gene Nupr1 impairs PanIN formation by modulating Kras G12D-induced senescence. *Cell Death Differ* **21**, 1633–1641.
- Emma MR, Iovanna JL, Bachvarov D, Puleio R, Loria GR, Augello G, Candido S, Libra M, Gulino A & Cancila V (2016) NUPR1, a new target in liver cancer: implication in controlling cell growth, migration, invasion and sorafenib resistance. *Cell Death Dis* **7**, e2269.
- Giroux V, Malicet C, Barthet M, Gironella M, Archange C, Dagorn J-C, Vasseur S & Iovanna JL (2006) p8 is a new target of gemcitabine in pancreatic cancer cells. *Clin Cancer Res* **12**, 235–241.
- Hamidi T, Cano CE, Grasso D, Garcia MN, Sandi MJ, Calvo EL, Dagorn J-C, Lomberg G, Urrutia R, Goruppi S *et al.* (2012) Nupr1-aurora kinase A pathway provides protection against metabolic stress-mediated autophagic-associated cell death. *Clin Cancer Res* **18**, 5234–5246.
- Averous J, Lambert-Langlais S, Cherasse Y, Carraro V, Parry L, B'chir W, Jousse C, Maurin AC, Bruhat A & Fafournoux P (2011) Amino acid deprivation regulates the stress-inducible gene p8 via the GCN2/ATF4 pathway. *Biochem Biophys Res Commun* **413**, 24–29.
- Garcia-Montero A, Vasseur S, Mallo GV, Soubeyran P, Dagorn JC & Iovanna JL (2001) Expression of the stress-induced p8 mRNA is transiently activated after culture medium change. *Eur J Cell Biol* **80**, 720–725.
- Barbosa-Sampaio HC, Liu B, Drynda R, De Ledsma AMR, King AJ, Bowe JE, Malicet C, Iovanna JL, Jones PM & Persaud SJ (2013) Nupr1 deletion protects against glucose intolerance by increasing beta cell mass. *Diabetologia* **56**, 2477–2486.
- Clark DW, Mitra A, Fillmore RA, Jiang WG, Samant RS, Fodstad O & Shevde LA (2008) NUPR1 interacts with p53, transcriptionally regulates p21 and rescues breast epithelial cells from doxorubicin-induced genotoxic stress. *Curr Cancer Drug Targets* **8**, 421–430.
- Hamidi T, Cano CE, Grasso D, Garcia MN, Sandi MJ, Calvo EL, Dagorn J-C, Lomberg G, Goruppi S, Urrutia R *et al.* (2013) NUPR1 works against the metabolic stress-induced autophagy-associated cell death in pancreatic cancer cells. *Autophagy* **9**, 95–97.
- Taïeb D, Malicet C, Garcia S, Rocchi P, Arnaud C, Dagorn J, Iovanna JL & Vasseur S (2005) Inactivation of stress protein p8 increases murine carbon tetrachloride hepatotoxicity via preserved CYP2E1 activity. *Hepatology* **42**, 176–182.
- Schönthal AH (2012) Endoplasmic reticulum stress: its role in disease and novel prospects for therapy. *Scientifica (Cairo)* **2012**, 857516.
- Kubisch CH & Logsdon CD (2008) Endoplasmic reticulum stress and the pancreatic acinar cell. *Expert Rev Gastroenterol Hepatol* **2**, 249–260.
- Ron D & Walter P (2007) Signal integration in the endoplasmic reticulum unfolded protein response. *Nat Rev Mol cell Biol* **8**, 519.
- Chambers JE, Dalton LE, Clarke HJ, Malzer E, Dominicus CS, Patel V, Moorhead G, Ron D & Marciniak SJ (2015) Actin dynamics tune the integrated stress response by regulating eukaryotic initiation factor 2 α dephosphorylation. *Elife* **4**, e04872.
- Livezey M, Huang R, Hergenrother PJ & Shapiro DJ (2018) Strong and sustained activation of the anticipatory unfolded protein response induces necrotic cell death. *Cell Death Differ* **25**, 1796–1807.
- Kato H & Nishitoh H (2015) Stress responses from the endoplasmic reticulum in cancer. *Front Oncol* **5**, 93.
- Santofimia-Castaño P, Lan W, Bintz J, Gayet O, Carrier A, Lomberg G, Neira JL, González A, Urrutia R, Soubeyran P *et al.* (2018) Inactivation of NUPR1 promotes cell death by coupling ER-stress responses with necrosis. *Sci Rep* **8**, 16999.

- 19 Cai D, Huang E, Luo B, Yang Y, Zhang F, Liu C, Lin Z, Xie W-B & Wang H (2016) Nupr1/Chop signal axis is involved in mitochondrion-related endothelial cell apoptosis induced by methamphetamine. *Cell Death Dis* **7**, e2161.
- 20 Bertolotti A, Zhang Y, Hendershot LM, Harding HP & Ron D (2000) Dynamic interaction of BiP and ER stress transducers in the unfolded-protein response. *Nat Cell Biol* **2**, 326–332.
- 21 Harding HP, Zhang Y, Zeng H, Novoa I, Lu PD, Calfon M, Sadri N, Yun C, Popko B & Paules R (2003) An integrated stress response regulates amino acid metabolism and resistance to oxidative stress. *Mol Cell* **11**, 619–633.
- 22 Marciniak SJ, Yun CY, Oyadomari S, Novoa I, Zhang Y, Jungreis R, Nagata K, Harding HP & Ron D (2004) CHOP induces death by promoting protein synthesis and oxidation in the stressed endoplasmic reticulum. *Genes Dev* **18**, 3066–3077.
- 23 Kramer R, Weber TK, Arceci R, Ramchurren N, Kastriakis WV, Steele G Jr & Summerhayes IC (1995) Inhibition of N-linked glycosylation of P-glycoprotein by tunicamycin results in a reduced multidrug resistance phenotype. *Br J Cancer* **71**, 670.
- 24 Reid DW, Chen Q, Tay AS-L, Shenolikar S & Nicchitta CV (2014) The unfolded protein response triggers selective mRNA release from the endoplasmic reticulum. *Cell* **158**, 1362–1374.
- 25 Sicari D, Delaunay-Moisán A, Combettes L, Chevet E & Igaría A (2019) A guide to assessing endoplasmic reticulum homeostasis and stress in mammalian systems. *FEBS J* **287**, 27–42.
- 26 Schuck S, Prinz WA, Thorn KS, Voss C & Walter P (2009) Membrane expansion alleviates endoplasmic reticulum stress independently of the unfolded protein response. *J Cell Biol* **187**, 525–536.
- 27 Kubisch CH & Logsdon CD (2007) Secretagogues differentially activate endoplasmic reticulum stress responses in pancreatic acinar cells. *Am J Physiol Liver Physiol* **292**, G1804–G1812.
- 28 Mayerle J, Sendler M & Lerch MM (2013) Secretagogue (Caerulein) induced pancreatitis in rodents. *Pancreapedia Exocrine Pancreas Knowl Base*.
- 29 Santofimia-Castaño P, Xia Y, Lan W, Zhou Z, Huang C, Peng L, Soubeyran P, Velázquez-Campoy A, Abián O, Rizzuti B *et al.* (2019) Ligand-based design identifies a potent NUPR1 inhibitor exerting anticancer activity via necroptosis. *J Clin Invest* **129**, 2500–2513.
- 30 Liu J, Xu Y, Stoleru D & Salic A (2012) Imaging protein synthesis in cells and tissues with an alkyne analog of puromycin. *Proc Natl Acad Sci USA* **109**, 413–418.
- 31 Chowdhury UR, Samant RS, Fodstad O & Shevde LA (2009) Emerging role of nuclear protein 1 (NUPR1) in cancer biology. *Cancer Metastasis Rev* **28**, 225–232.
- 32 Kojima E, Takeuchi A, Haneda M, Yagi F, Hasegawa T, Yamaki K, Takeda K, Akira S, Shimokata K & Isobe K (2003) The function of GADD34 is a recovery from a shutoff of protein synthesis induced by ER stress—elucidation by GADD34-deficient mice. *FASEB J* **17**, 1–18.
- 33 Vasseur S, Hoffmeister A, Garcia-Montero A, Mallo GV, Feil R, Kühbandner S, Dagorn J-C & Iovanna JL (2002) p8-deficient fibroblasts grow more rapidly and are more resistant to adriamycin-induced apoptosis. *Oncogene* **21**, 1685–1694.
- 34 Chirgwin JM, Przybyla AE, MacDonald RJ & Rutter WJ (1979) Isolation of biologically active ribonucleic acid from sources enriched in ribonuclease. *Biochemistry* **18**, 5294–5299.
- 35 Salic A & Mitchison TJ (2008) A chemical method for fast and sensitive detection of DNA synthesis *in vivo*. *Proc Natl Acad Sci USA* **105**, 2415–2420.
- 36 Shevchenko Andrej, Tomas Henrik, Havli Jan, Olsen Jesper V, Mann Matthias (2006) In-gel digestion for mass spectrometric characterization of proteins and proteomes. *Nat Protoc* **1**, 2856–2860. <https://doi.org/10.1038/nprot.2006.468>
- 37 Bonacci T, Audebert S, Camoin L, Baudelet E, Bidaut G, Garcia M, Witzel I-I, Perkins ND, Borg J-P & Iovanna J-L (2014) Identification of new mechanisms of cellular response to chemotherapy by tracking changes in post-translational modifications by ubiquitin and ubiquitin-like proteins. *J Proteome Res* **13**, 2478–2494.

Supporting information

Additional supporting information may be found online in the Supporting Information section at the end of the article.

Tables S1–S3. NUPR1 interacting partners.

Table S4. String analysis.

Data S1. Nup1-IP-Flag analysis.